AIAA JOURNAL
Vol. 47, No. 1, January 2009

Extremum-Seeking Control of Subsonic Cavity Flow

Kihwan Kim,* Coşku Kasnakoğlu,† Andrea Serrani,‡ and Mo Samimy§
The Ohio State University, Columbus, Ohio 43235

DOI: 10.2514/1.38180

An adaptive control system using extremum-seeking optimization is developed to suppress subsonic cavity flow resonance. First, a simple but effective linear feedback control law is employed. This control law uses pressure fluctuations measured at two different cavity side-wall locations as feedback signals. The influence of the control parameters (namely, a gain K and a phase shift ϕ) on the magnitude of the limit cycle in closed loop is investigated analytically and experimentally. Second, an extremum-seeking algorithm is implemented to optimize in real time the selection of the most critical control parameter ϕ in such a way that the magnitude of the limit cycle is minimized in closed loop. The performance of the resulting control system is compared with that of a linear-quadratic feedback controller of fixed structure, developed on the basis of a reduced-order model of cavity flow dynamics. Experimental results highlight the advantage of parameter adaptation provided by the extremum-seeking algorithm over the controller of fixed structure under varying flow conditions.

Nomenclature

b_j = constants in the simplified Galerkin system, $j = 1, 2$
C = linear transform matrix, $\in \mathbb{R}^{2\times 2}$
F_j = system matrices in the Galerkin system, $j = 1, 2$
G_{BP} = bandpass filter
G_j = system matrices in the Galerkin system, $j = 1, 2$
G_L = low-pass filter for limit cycle detection
K = control parameter corresponding to gain
k_j = control parameters in the η coordinates, $j = 1, 2$
P_j = local pressure fluctuations measured inside a cavity, $j = 1, \ldots, 6$
p = pressure—a pair of pressure measurements (p_a, p_b) used as feedback signals
R_{ij} = normalized cross-correlation estimate of the pressure signals P_i and P_j
u = control input, $\in \mathbb{R}$
α = constant in the simplified Galerkin system, $\in \mathbb{R}$
β = constant in the simplified Galerkin system, $\in \mathbb{R}$
ζ = state variables of the Galerkin system representing transient dynamics
η = state variables of the Galerkin system representing oscillatory dynamics
θ = state variable in polar coordinates representing phase
ρ = state variable in polar coordinates representing magnitude
$\bar{\rho}$ = averaged magnitude of the limit cycle
$\bar{\rho}_o$ = averaged magnitude of the limit cycle for baseline flows
ρ^* = magnitude of the limit cycle
$\rho^*_{\min}$ = minimized magnitude of the limit cycle
σ = constant in the simplified Galerkin system, $\in \mathbb{R}$
ϕ = control parameter corresponding to phase
ϕ_{opt} = optimal value of ϕ
ω_a = perturbation frequency for extremum-seeking control
ω_h = high-pass filter cutoff frequency for extremum-seeking control
ω_L = cutoff frequency for limit cycle detection
ω_l = low-pass filter cutoff frequency for extremum-seeking control

Presented as Paper 0281 at the 46th AIAA Aerospace Science Meeting, Reno, Nevada, 7–10 January 2008; received 21 April 2008; revision received 17 August 2008; accepted for publication 18 August 2008.

*Post Doctoral Researcher, Department of Electrical and Computer Engineering and Department of Mechanical Engineering; currently with POSCO Technical Research Laboratories, POSCO, Korea; kihwank@posco.com. Member AIAA.

†Graduate Student, Department of Electrical and Computer Engineering; currently with Department of Electrical and Electronics Engineering, TOBB University of Economics and Technology, Turkey; kasnakoglu@etu.edu.tr

‡Associate Professor, Department of Electrical and Computer Engineering; serrani@ece.osu.edu. Member AIAA.

§The Howard D. Winbigler Professor of Engineering, Director of Gas Dynamics and Turbulence Laboratory, Department of Mechanical Engineering; samimy.1@osu.edu. Associate Fellow AIAA.

I. Introduction

CLOSED-LOOP flow control is regarded as the most effective method to stabilize and improve the performance of fluid systems with minimized actuation efforts under varying operating conditions [1]. In particular, cavity flow control has been the subject of intense investigation for many years, due to its importance in aerodynamic applications. Flow over a shallow cavity produces self-sustained oscillations that result from the coupling between flow dynamics and flow-induced acoustic field [2]. These oscillations lead to strong resonant tones, which are known to cause, among other effects, structural damages on the mechanical systems that interact with the flow. Flow control applied to cavity flow systems aims at formulating strategies for suppressing or reducing the amplitude of the acoustic tones [3,4].

In the past few years, the flow control group at The Ohio State University has developed and experimentally validated several approaches to feedback control for subsonic cavity flow oscillations. An open-loop actuation scheme updated by a logic-based feedback law was originally proposed by Debiasi and Samimy [5]. Subsequently, a parallel-proportional controller with time delay [6] and a neural-network approach [7] showed promising performances in attenuating cavity flow resonance. More recently, major advances have been achieved by employing a linear-quadratic (LQ) controller designed on the basis of an experimentally derived reduced-order flow model [2].

In many applications, the goal of a feedback control system is to regulate certain output variables to optimize a given cost function. Occasionally, the characteristics of the cost function change depending on internal conditions and the external environment. Such uncertainties in the cost function necessitate the use of adaptive algorithms to iteratively search for the optimal input such that the performance output can be minimized. A control strategy that embeds a self-tuning mechanism to track a varying minimum of the cost function is termed *extremum-seeking (ES) control* [8]. Some advantages of extremum-seeking control over controllers of fixed structure can be summarized as follows:

1) The application of extremum-seeking control does not require, in principle, a detailed control-oriented model of the plant. This is a particularly useful feature for dynamic systems of interest described by complex and/or uncertain models.

2) ES control can be applied to a large class of nonlinear systems.

3) ES control can be readily implemented in real-time applications, due to the relative simplicity of the tuning algorithm.

Extremum-seeking control has been of great practical interest since the 1950s and 1960s [9]. Recently, the implementation of this control scheme has been actively pursued for various industrial systems, for example, in maximum power point tracking of photovoltaic arrays [10], pointing control for intersatellite laser communications [11], performance improvement of antilock brake systems [12], power control of thermoacoustic coolers [13], parameter optimization of dual-independent variable cam timing engines [14], and control of combustion instibility [15]. Moreover, extremum-seeking control has already been investigated experimentally in a variety of flow-related configurations, including axial-flow compressors [16], diffuser [17], backward-facing step [18], bluff body [19,20], and airfoil [21].

In this research, a control system including an extremum-seeking algorithm is developed for suppressing subsonic cavity flow resonance. The magnitude of the limit cycle, computed from two pressure fluctuation measurements, is employed as the performance output of the system. A simple but effective feedback control law characterized on the basis of a simplified Galerkin system, which was originally proposed by Tadmor et al. [22] and previously used by Rowley and Juttijudata [23], is adopted as a baseline controller. The static input–output map of the closed-loop system between the controller parameters and the amplitude of the limit cycle in steady state is derived analytically and identified experimentally. Then, an extremum-seeking feedback loop is applied on the closed-loop control system, thereby optimizing the parameters of the controller in real time. As for the extremum-seeking scheme, the strategy implemented in this study follows closely the limit cycle minimization method presented by Wang and Krstić [24]. The extremum-seeking control is tested experimentally under different modes of cavity flow oscillation, that is, single and multimode resonances, such that its capability to adapt to different flow conditions is investigated.

The paper is organized as follows: In Sec. II, the experimental setup is described and the baseline characteristics of the cavity flow are explained. In Sec. III, a feedback control law, which corresponds to the inner loop of the overall control system, is proposed. The effect of the control parameters on the system performance in closed-loop operation are examined analytically and experimentally. Sections IV and V present, respectively, the experimental implementation of an extremum-seeking algorithm, and a comparative evaluation of its performance at various Mach numbers with that provided by the LQ feedback flow controller developed by Samimy et al. [2]. Concluding remarks are given in Sec. VI.

II. Experimental Setup

A blow-down wind tunnel, located at the Gas Dynamics and Turbulence Laboratory of The Ohio State University, is used for the experiments in this research. The tunnel can operate in the subsonic range between Mach 0.20 and Mach 0.70. Flow is directed to the 50.8 mm × 50.8 mm test section through a converging nozzle before exhausting to the atmosphere. As shown in Fig. 1, a shallow cavity is recessed in the test section with a depth $D = 12.7$ mm and length $L = 50.8$ mm ($L/D = 4$). The synthetic-jetlike actuator is connected to the leading edge of the cavity. The actuator consists of a Selenium D3300Ti compression driver linked to a 108-mm-long nozzle, which converges from the driver to an exit slot of width 1 mm. The diaphragm movement of the compression driver creates oscillatory flow that exits through the slot at an angle of 30 deg with respect to the freestream flow. The pressure fluctuations are measured at six locations on the side wall of the cavity by flush-mounted XCL-100-25A transducers. The signals pass through an antialiasing filter with a 10-kHz cutoff frequency. A dSpace 1103 DSP board operating at a 50-kHz sampling rate is used to manage the data acquisition and the implementation of feedback control algorithms. Further details on the experimental setup and the actuator characteristics can be found in Debiasi and Samimy [5] and Kim et al. [25].

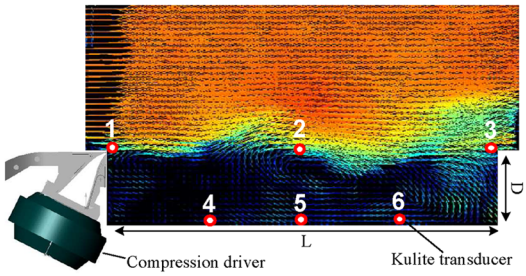

Fig. 1 Schematic of the cavity with superimposed velocity vectors and magnitude obtained using particle image velocimetry for baseline flow at Mach 0.30. The locations of six pressure transducers are also shown.

The characteristics of the experimental setup have been thoroughly investigated in previous work [2,5]. At Mach 0.3, the cavity flow shows a time-invariant, single-mode resonance corresponding to the third Rossiter mode. This flow condition exhibits rather simple characteristics compared with other multiresonance modes, thereby facilitating the development of the single-parameter extremum-seeking control being pursued in this research. The previously developed LQ control system [2], which is compared with the extremum-seeking control in Sec. V, was also developed at Mach 0.30. Therefore, the cavity flow at Mach 0.3 is selected as a reference baseline for this research. However, the extremum-seeking controller is further examined at various Mach numbers, including Mach numbers corresponding to a multi-resonance mode, in order to assess its adaptability to varying flow conditions. In this cavity configuration, the resonance peaks occur within 2–4 kHz regardless of resonance mode [2]. Therefore, this range is considered hereafter as a frequency range of interest for control system design.

III. Simple Feedback Controller for Cavity Flow Oscillation

In this section, a simple feedback law is derived for a closed-loop control system to suppress cavity flow oscillation. This control law is based on a phasor model, obtained from a simplified Galerkin system representing a reduced-order flow model. The type of controller employed in this study was originally proposed by Tadmor et al. [22] in the context of suppressing cylinder wake instability, and later considered by Rowley and Juttijudata [23] for cavity flows. The performance of the proposed control system is experimentally verified and compared with analytic results.

A. Theoretical Analysis

A reduced-order model of cavity flow, derived by means of proper orthogonal decomposition and Galerkin projection techniques [2], can be written in modal coordinates as

$$\begin{aligned}\dot{\eta} &= F_1\eta + \varphi_1(\eta,\zeta) + (G_1 + \gamma_1(\eta,\zeta))u \\ \dot{\zeta} &= F_2\zeta + \varphi_2(\eta,\zeta) + (G_2 + \gamma_2(\eta,\zeta))u\end{aligned} \tag{1}$$

where $u \in \mathbb{R}$ stands for the control input,

$$\eta = \begin{pmatrix}\eta_1 \\ \eta_2\end{pmatrix}, \qquad \zeta = \begin{pmatrix}\zeta_1 \\ \vdots \\ \zeta_{N-2}\end{pmatrix}, \qquad F_1 = \begin{bmatrix}\sigma & -\omega \\ \omega & \sigma\end{bmatrix}$$

$$F_2 = \mathrm{diag}(-\lambda_1, \ldots, -\lambda_{N-2})$$

$G_1 \in \mathbb{R}^2$, $G_2 \in \mathbb{R}^{N-2}$, $\varphi_1, \gamma_1 : \mathbb{R}^2 \times \mathbb{R}^{N-2} \to \mathbb{R}^2$, $\varphi_2, \gamma_2 : \mathbb{R}^2 \times \mathbb{R}^{N-2} \to \mathbb{R}^{N-2}$, and $\sigma > 0$, $\omega > 0$, $\lambda_i > 0$, $i = 1, \ldots, N$. In this

Galerkin system, the state variable ζ accounts for fast transient dynamics, while the state η describes oscillatory behavior of the system. Elimination of ζ from Eq. (1) by means of center-manifold reduction [26] leads to a simple model of cavity flow oscillation as

$$\dot{\eta} = \begin{bmatrix} \sigma - \alpha\rho^2 & -\omega - \beta\rho^2 \\ \omega + \beta\rho^2 & \sigma - \alpha\rho^2 \end{bmatrix} \eta + \begin{pmatrix} b_1 \\ b_2 \end{pmatrix} u$$
$$\text{where } \alpha > 0 \quad \text{and} \quad \rho = \sqrt{\eta_1^2 + \eta_2^2} \tag{2}$$

Using polar coordinates ρ and $\theta = \tan^{-1}(\eta_2/\eta_1)$, system Eq. (2) is transformed into the phasor model [22,23]

$$\dot{\rho} = (\sigma - \alpha\rho^2)\rho + (b_1 \cos\theta + b_2 \sin\theta)u \tag{3a}$$

$$\dot{\theta} = \omega + \beta\rho^2 + \frac{1}{\rho}(b_2 \cos\theta - b_1 \sin\theta)u \tag{3b}$$

where it is readily seen that, when $u = 0$, the magnitude ρ converges to a stable equilibrium $\rho^* = \sqrt{\sigma/\alpha}$, which corresponds to the magnitude of a stable limit cycle in the original coordinates η.

Compared with the original system in Eq. (1), the model in Eq. (3) omits detailed dynamics of cavity flow oscillation. However, it still preserves some of the key characteristics related to the limit cycle oscillation of the original model and could be used to design a simple feedback controller [23]. To this end, consider the linear control law

$$u = -k_1\eta_1 - k_2\eta_2 = -K\rho\cos(\theta - \phi) \tag{4}$$

where $K = \sqrt{k_1^2 + k_2^2} > 0$ and $\phi = \tan^{-1}(k_2/k_1) \in [0, 2\pi)$. After application of this control law, averaging of Eq. (3a) with respect to $\theta \in [0, 2\pi)$ yields [23]

$$\dot{\rho} = (\sigma - \alpha\rho^2)\rho - K\rho(b_1 \cos\phi + b_2 \sin\phi) \tag{5}$$

The averaging theorem [27] allows an approximation of the solution of Eq. (5) with the solution of Eq. (3a). The effect of the control law in Eq. (4) on the magnitude of the limit cycle is to change ρ^* from $\sqrt{\sigma/\alpha}$ to

$$\rho^* = \sqrt{\frac{\sigma - K(b_1 \cos\phi + b_2 \sin\phi)}{\alpha}} \tag{6}$$

where it is assumed that the magnitude of the control gain K is small enough to preserve the oscillation, that is, $K(b_1 \cos\phi + b_2 \sin\phi) < \sigma$. Note that the control u in Eq. (4) contains in principle 2 degrees of freedom, that is, K and ϕ, which can be used for parameter optimization. As noted by Rowley and Juttijudata [23] and Tadmor et al. [22], for each K, tuning the phase ϕ to the optimal value ϕ_{opt} satisfying

$$\cos\phi_{\text{opt}} = b_1/|b|,$$
$$\sin\phi_{\text{opt}} = b_2/|b|, \quad \text{where } |b| = \sqrt{b_1^2 + b_2^2}$$

has the effect of minimizing ρ^* to the value

$$\rho^*_{\min} = \sqrt{\frac{\sigma - K|b|}{\alpha}} \tag{7}$$

From Eq. (7), it is seen that increasing the gain K to become larger than $\sigma/|b|$ eventually forces the limit cycle oscillation to vanish, that is, $\rho^*_{\min} \to 0$. This analytic result is, in general, different from what is observed in experiments, where complete suppression of oscillation cannot be achieved by applying the control law in Eq. (4). This is not surprising, because the analysis is based on a simplified reduced-order model which only captures the behavior of the system to a limited extent. Therefore, the characteristics of the proposed closed-loop control need to be assessed by using cavity flow experiments. Unfortunately, it is not viable to implement the control law in Eq. (4) directly in the cavity flow configuration, because the state variables η cannot be measured in real time from the flowfield. Alternatively, provided that a linear relationship of the form

$$p = C\eta, \qquad C \in \mathbb{R}^{2\times 2}$$

exists between η and a pair of local pressure measurements $p = (p_a, p_b)^T$, it is possible to reformulate Eq. (4) as

$$u = -K\rho\cos(\theta - \phi) = -\begin{bmatrix} k_1 & k_2 \end{bmatrix} C^{-1} p = -\tilde{K}\,\tilde{\rho}\cos(\tilde{\theta} - \tilde{\phi}) \tag{8}$$

where $\tilde{\rho} = \sqrt{p_a^2 + p_b^2}$ and $\tilde{\theta} = \arctan(p_b/p_a)$. Note that the control law in Eq. (8) has exactly the same structure as the original controller in Eq. (4). Therefore, the same control strategy can be implemented in terms of feedback from independent pressure measurements instead of state variables. Obviously, for any given flow configuration, the actual computation of the parameters $(\tilde{K}, \tilde{\phi})$ requires knowledge of the plant model parameters, including the output map C, which are affected by a large uncertainty due to the approximate nature of the phasor model (3). However, this limitation will be overcome by a self-tuning mechanism embedded in the control scheme, as discussed in Sec. IV. For the sake of convenience, the notation $(\tilde{\cdot})$ will be omitted for the remainder of the paper, with an understanding that the controller parameters refer to Eq. (8).

B. Experimental Verification

The state variables η_1 and η_2 in Eq. (4) describe the system dynamics associated with the limit cycle oscillation. Therefore, the two signals p_a and p_b in Eq. (8) should possess the same dynamic characteristics as the state η. As shown in Fig. 1, pressure fluctuation signals are measured at six locations on the walls of the cavity. The rationale behind the selection of the two best signals among the available pressure measurements is based on the following criteria:

1) The signal-to-noise (S/N) ratio of the selected signals should be the largest possible. The S/N ratios of each pressure signal can be examined graphically from the sound-pressure-level (SPL) spectra, by comparing the magnitude of the resonance peak with the background noise level.

2) The two selected signals should be strongly correlated. The normalized form of the cross-correlation estimate indicating the similarity between two real-valued signals can be computed from N samples of the signals u and v as [28]

$$R_{uv}(m) = \frac{1}{\sqrt{R_{uu}(0)R_{vv}(0)}} \cdot \begin{cases} \sum_{n=0}^{N-m-1} u[n+m]v[n], & m \geq 0 \\ R_{vu}(-m), & m < 0 \end{cases} \tag{9}$$

where $-N + 1 \leq m \leq N - 1$, and the values $R_{uu}(0)$ and $R_{vv}(0)$ stand for the autocorrelations of the signals u and v at $m = 0$, respectively.

Figure 2a presents the SPL spectra of the pressure fluctuations, which are denoted by $P_j (j = 1 \cdots 6)$ for each location in Fig. 1. The pressures are measured at baseline Mach 0.30 flow. The magnitudes of the resonance peaks are similar for all the pressure fluctuations P_i except P_1, whereas the background noise levels of each fluctuation vary between 100 and 120 dB. The background noise levels of P_1 to P_3 at the shear layer are higher than those of P_4 to P_6 at the bottom of the cavity. Therefore, the signals P_4 to P_6 perform better than the signals P_1 to P_3 in terms of S/N ratio, as defined by the magnitude of resonance peak with respect to background noise level. The cross-correlation analysis is performed for all possible 15 pairs resulting from the six pressure measurements. Figure 2b shows the worst and best results obtained from the correlation analysis. Compared with the worst cross correlation R_{23} from the pressure pair (P_2, P_3), the best cross correlation R_{45} from the pair (P_4, P_5) exhibits a strong oscillation that is a typical characteristic of two signals describing periodic orbits in the phase space. Based on these criteria, the pair (P_4, P_5) is selected as feedback (p_a, p_b) for the controller in Eq. (8).

Figure 3 shows the diagram of closed-loop control experiments using the proposed control law. To minimize the effects of background noise, the feedback signals P_4 and P_5 are filtered by a

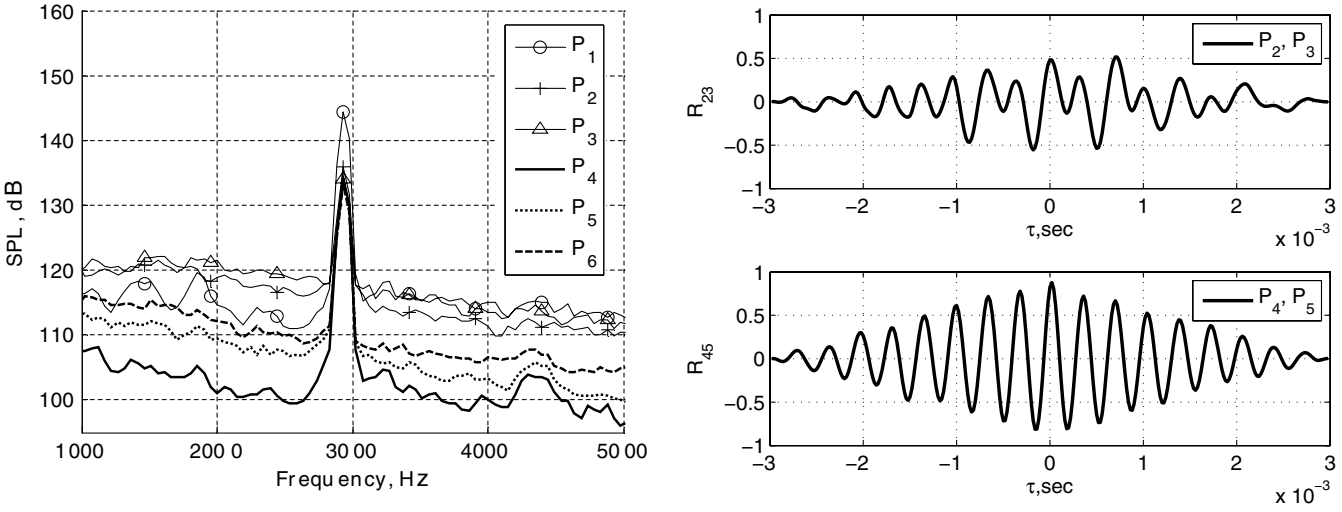

a) SPL spectra from the wall pressure measurements

b) Cross-correlation for (P_2, P_3) and (P_4, P_5)

Fig. 2 Characteristics of wall pressure fluctuations at Mach 0.30 baseline flow.

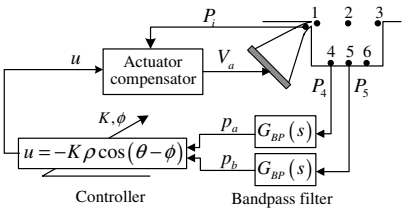

Fig. 3 Inner-loop feedback control system.

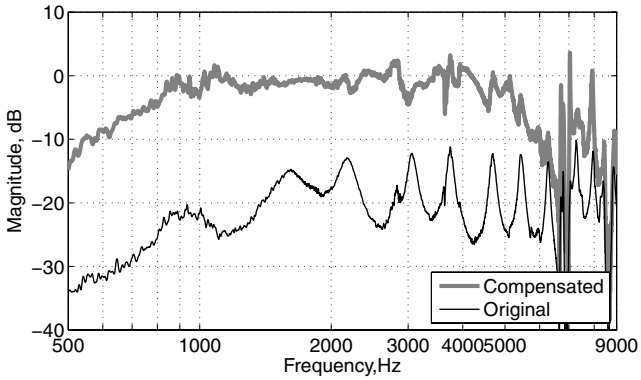

Fig. 4 Frequency responses of the original (black) and compensated (gray) actuator dynamics (from Kim et al. [25]).

pair of fourth-order Butterworth bandpass filters, $G_{\mathrm{BP}}(s)$, having a passband of 1.5–4 kHz. In addition, the actuator compensator described by Kim et al. [25] is embedded in the control loop. The synthetic jetlike actuator employed in the experimental setup possesses its own dynamic characteristics, which result from the geometric features of the converging nozzle guiding the actuator output to the cavity. The actuator dynamics severely distorts the control signal u, thereby deteriorating the overall control performance. The actuator compensator forces the actuator output pressure P_i, which is measured at the exit slot, to accurately track the desired control input u by providing a feedback control that commands the voltage signal V_a to the actuator. For the compensator design, a time-delay model of the actuator dynamics was obtained using subspace-based identification methods from the experimental data. Based on the identified actuator model, a 2-degree-of-freedom Smith-predictor–type control structure was employed in conjunction with a H_∞ mixed-sensitivity method. As a result of the application of the compensator, the uncertainty caused by the actuator dynamics is effectively mitigated, and its effect can be ignored in assessing the overall closed-loop performance. This objective is achieved by increasing the gain and decreasing the fluctuation of the frequency response, as shown in Fig. 4.

The closed-loop system shown in Fig. 3 allows us to identify the static map between the control parameters (K, ϕ), which are manually tuned, and the limit cycle magnitude ρ^*. For this purpose, the gain K is changed from 0.5 to 1.7 with a resolution of $\Delta K = 0.2$, while the phase is increased from 0 to 2π with a resolution of $\Delta\phi = 0.3$ rad. For each pair of control parameter values, the corresponding averaged amplitude of the oscillation $\bar{\rho}$ is computed in steady state. The experiments are performed at Mach 0.30. A plot of $\bar{\rho}$ versus the controller parameters (K, ϕ) is shown in Fig. 5, where the magnitude $\bar{\rho}$ is normalized by the averaged limit cycle magnitude of the baseline flow, $\bar{\rho}_o = 0.36$ kPa. It is observed from Fig. 5a that the experimental results are in good agreement with the analysis in Eq. (6) as far as the variation of the phase shift parameter ϕ is concerned, since there exists an optimal value $\phi_{\mathrm{opt}} = 5.4$ rad for this controller parameter where $\bar{\rho}$ is minimized, irrespective of the value of K in the given range. However, as shown in Fig. 5b, the effect of the variation of K does not match the analytical model. As K increases while ϕ is fixed at 5.4, the magnitude $\bar{\rho}$ decreases below 37% of the baseline magnitude, but tends to increase again when $K > 1.5$. Conversely, Eq. (7) predicts a monotonic attenuation of the limit cycle magnitude with increasing K when ϕ is set to the optimal value ϕ_{opt}. This result implies that the simple averaged model in Eq. (5) leads to a considerable discrepancy between the real effect of K on ρ^*_{min} and the analytical relationship in Eq. (7).

Figure 6 shows the performance of the control system corresponding to $K = 1.0$, $\phi = 5.4$, which is hereby regarded as an optimal parameter set. The phase plot in Fig. 6a shows that the limit cycle magnitude of the controlled flow is substantially decreased, compared with that of the baseline flow. As seen from the SPL spectra shown in Fig. 6b, the controller reduces the resonance peak by 22 dB with respect to the baseline case.

IV. Extremum-Seeking Optimization of Control Parameters

The next step is the formulation of an adaptive extremum-seeking algorithm to tune the control parameters online. As mentioned earlier, the extremum-seeking scheme can have 2 degrees of freedom, corresponding to the parameters K and ϕ, for the optimization. However, adapting K will not be appropriate for the controller considered here due to the following reasons:

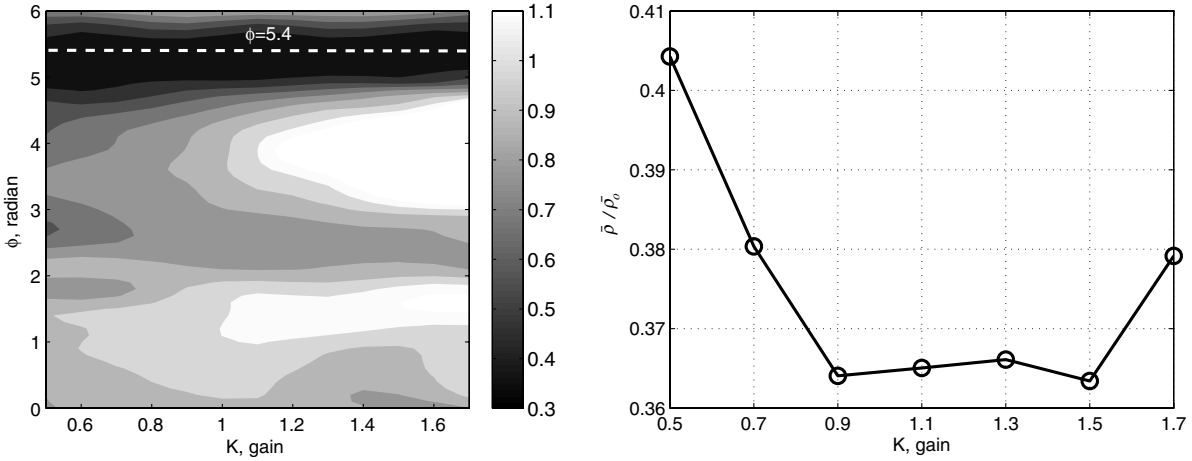

a) Averaged limit cycle magnitude, $\bar{\rho}/\bar{\rho}_o$ **b) Effect of K on $\bar{\rho}/\bar{\rho}_o$ at ϕ= 5.4**

Fig. 5 Variation of averaged limit cycle magnitude, $\bar{\rho}/\bar{\rho}_o$ ($\bar{\rho}_o = 0.36$ kPa), with respect to control parameters K and ϕ.

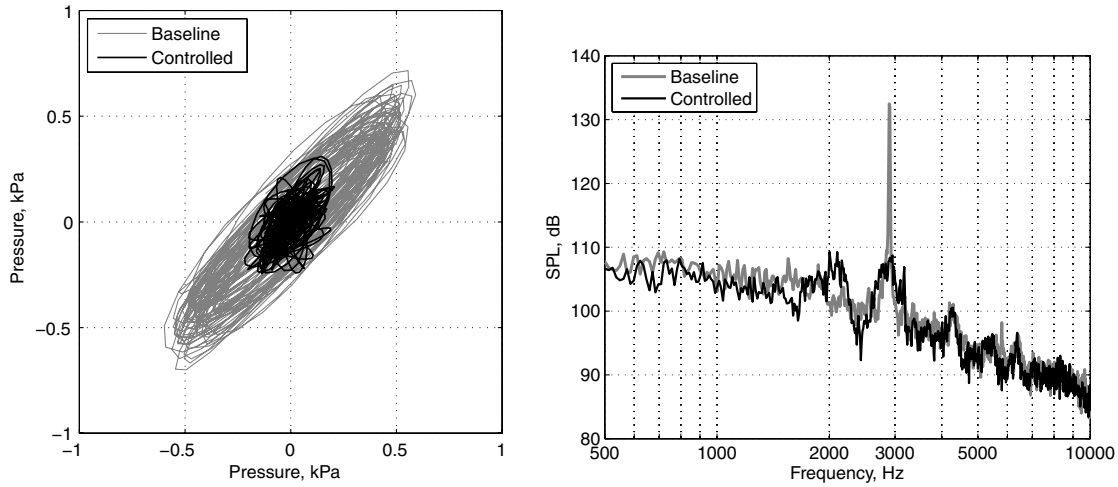

a) Phase plot. x axis: p_a and y axis: p_b **b) SPL spectra from the transducer 5 (P_5)**

Fig. 6 Performance of the closed-loop control with the control parameters $K = 1.0$ and $\phi = 5.4$ at Mach 0.30 flow.

1) Increasing K may cause actuator saturation, and thus its effect will be limited.

2) The sensitivity of ρ^* to the variation of K is much smaller than that of ϕ.

3) The phase shift ϕ determines the sign of the feedback action, and thus its effect is crucial in determining attenuation or amplification of the limit cycle.

These characteristics can be clearly observed in Fig. 5. Hence, the gain K is kept constant at $K = 1.0$ and only the phase ϕ is adapted in this study.

The structure of the single-parameter extremum-seeking optimization algorithm, adopted from Wang and Krstić [24], is shown in Fig. 7. The extremum-seeking controller acts as an outer loop to the controller in Fig. 3. The scheme implements an online gradient-based optimization, where the sensitivity of ρ^* with respect to ϕ is estimated by introducing a sinusoidal perturbation $\Delta\phi$. Subsequently, the parameter ϕ is adapted in real time using a gradient descent method to achieve the minimum of the limit cycle magnitude, ρ^*.

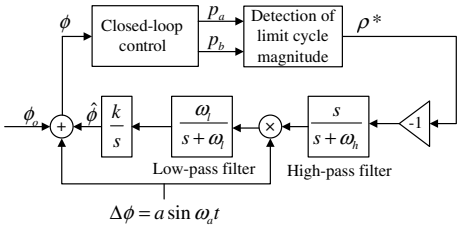

Fig. 7 Outer feedback loop using extremum-seeking algorithm.

Following Wang and Kristić [24], a detection algorithm for the limit cycle magnitude ρ^* can be readily established as follows: Assuming that $p_a = r_a \cos\omega t$ and $p_b = r_b \sin\omega t$, the magnitude of ρ^2 becomes

$$\rho^2 = p_a^2 + p_b^2 = \frac{(r_a^2 + r_b^2)}{2} + \frac{(r_a^2 - r_b^2)}{2}\cos 2\omega t \tag{10}$$

The signal ρ^2 is filtered through a low-pass filter $G_L(s)$. Provided that the bandwidth ω_L of $G_L(s)$ satisfies the condition $\omega_L \ll \omega$, the filter $G_L(s)$ allows the extraction of the time-invariant component from Eq. (10) as

$$\rho^* = \sqrt{\frac{1}{2}(r_a^2 + r_b^2)}$$

Suppose that the static input–output map f: $\phi \to \rho^*$ representing the relationship between ϕ and ρ^* has a minimum. In the vicinity of an initial value $\phi = \phi_o$, the map f can be approximated by Taylor series as

$$\rho^* = f(\phi) \approx f(\phi_o) + f'(\phi_o)\Delta\phi = f(\phi_o) + f'(\phi_o)a\sin(\omega_a t) \tag{11}$$

where $\Delta\phi = a\sin(\omega_a t)$, $a \ll O(\phi)$ is a perturbation signal. As shown in Fig. 7, the perturbation is implemented as an additive sinusoidal signal, whose frequency ω_a should be sufficiently low such that the static relationship $\rho^* = f(\phi)$ can be maintained. From Fig. 7, the bandwidths ω_h and ω_l of high-pass and low-pass filters, respectively, are chosen to satisfy the condition $\omega_h, \omega_l \ll \omega_a$. As a result, the update variable $\hat{\phi}$ in Fig. 7 is approximately related to the gradient of the f as follows:

$$\dot{\hat{\phi}} \approx -kf'(\phi_o)\frac{a^2}{2} \tag{12}$$

which allows the detection of the gradient $f'(\phi_o)$ without the exact knowledge of the map. The value of $\hat{\phi}$ is updated by integrating f' at every time step until ρ^* approaches the minimum where $f'(\phi) = 0$. For the sake of stable and effective extremum-seeking optimization [8], the following relationships should be established:

cavity oscillation frequency,

$\omega \gg$ cutoff frequency for limit cycle detection

$\omega_L \gg$ perturbation frequency

$\omega_a \gg$ filter frequencies, $\quad \omega_l,\ \omega_h$ (13)

In what follows, the selection of the parameters of the filters in the extremum-seeking loop is discussed based on the conditions given in Eq. (13). First of all, a third-order Butterworth low-pass filter with a cutoff frequency $\omega_L/2\pi = 50$ Hz is chosen for the filter G_L used to compute the limit cycle magnitude. Note that the designed cutoff frequency at 50 Hz is considerably lower than the frequency range of interest in cavity flow oscillation, that is, 2–4 kHz. To determine the perturbation frequency ω_a, ϕ is varied from 0 to 2π at a given frequency f_a as follows:

$$\phi = \pi + \pi\sin(\omega_a t), \qquad \omega_a = 2\pi f_a \tag{14}$$

and the effect of each f_a on the relationship between ρ^* and ϕ is analyzed. Note that the extremum-seeking loop is not active during this investigation. The result of the analysis is shown in Fig. 8, where the solid lines account for increasing values of ϕ from 0 to 2π, while the dashed lines account for decreasing values from 2π to 0. At $f_a = 4$ Hz, the relationship between ϕ and ρ^* is very similar to the characteristic of the averaged limit cycle magnitude shown in Fig. 5a, as it possesses a minimum around 1.5π–2π, although the minimum value is shifted slightly depending on the direction of varying ϕ. As the frequency f_a increases to 8 and 16 Hz, the relationship loses the key characteristic of the existence of a minimum value. Consequently, the perturbation signal is set as $\Delta\phi = 0.1\sin(2\pi \cdot 3 \cdot t)$, where the frequency is lower than 4 Hz and the amplitude is smaller than the order $\mathcal{O}(\phi) \approx 1$. Subsequently, both filter frequencies ω_h and ω_l are set at 0.4 Hz to satisfy the condition in Eq. (13).

The resulting extremum-seeking controller is tested at Mach 0.3 flow. As shown in Fig. 7, the phase $\phi\ (=\phi_o + \hat{\phi} + \Delta\phi)$ consists of three components: initial value ϕ_o, update $\hat{\phi}$, and perturbation $\Delta\phi$. Figure 9a shows the transition of $\phi_o + \hat{\phi}$ that excludes the perturbation signal $\Delta\phi$ from ϕ. The parameter adaptation begins at $t = 0$. The value of $\phi_o + \hat{\phi}$ is successfully updated from the initial value $\phi_o = 4.5$, where $\hat{\phi} = 0$, to the steady-state value $\phi_\infty = 5.35$, where the limit cycle magnitude ρ^* reaches its minimum value of about 0.15 kPa, as shown in Fig. 9b. The parameter value $\phi_\infty = 5.35$ is very close to $\phi_{\text{opt}} = 5.4$, the optimal value identified during the closed-loop experiments in Sec. III. This result verifies that the

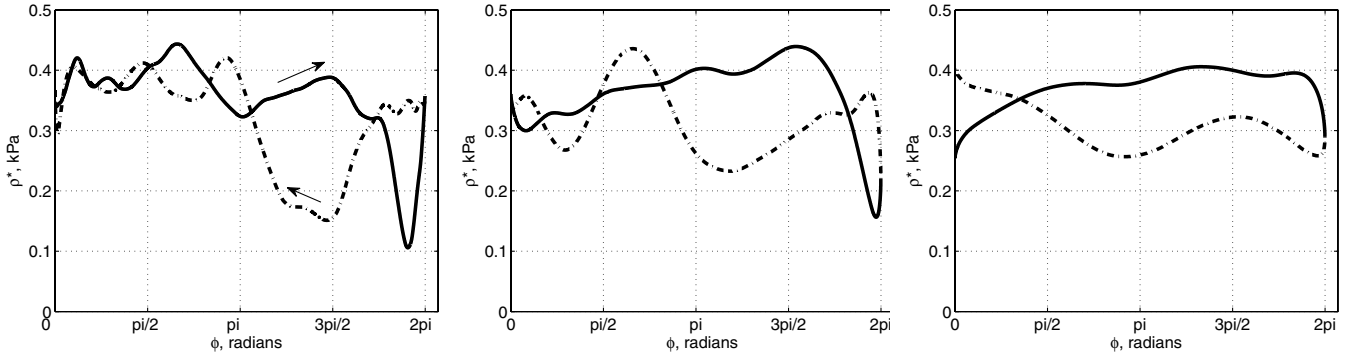

a) f_a = 4 Hz **b) f_a = 8 Hz** **c) f_a = 16 Hz**

Fig. 8 Effects of perturbation frequency f_a on the relationship between ρ^* and ϕ.

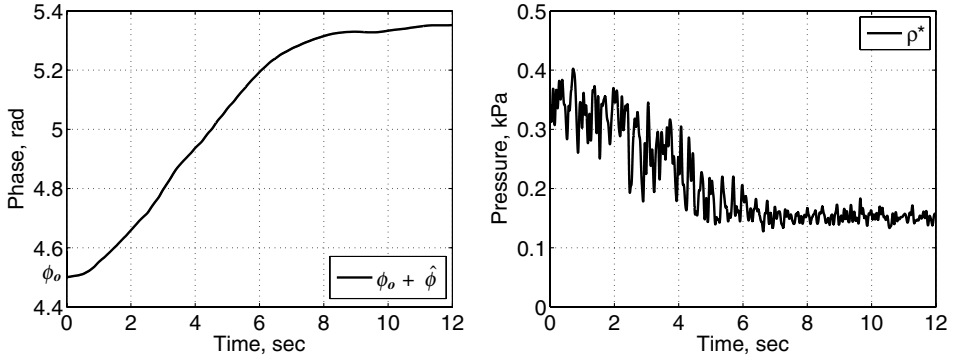

a) Control parameter ϕ **b) Limit cycle magnitude ρ^***

Fig. 9 Transient characteristics of the extremum-seeking control.

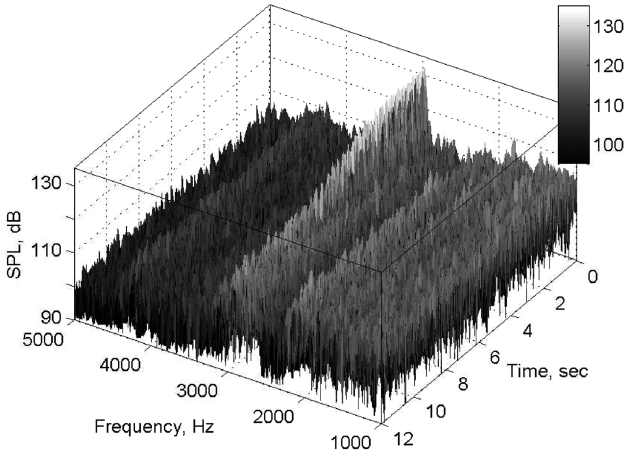

Fig. 10 SPL spectrogram from transducer 5 in transition under extremum-seeking (ES) control.

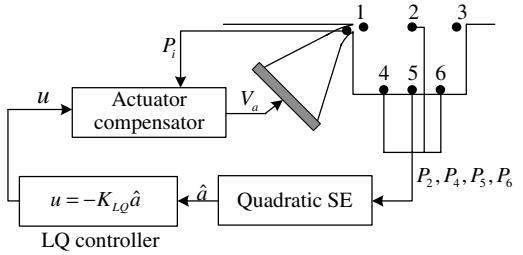

Fig. 11 Linear-quadratic feedback system for cavity flows. Pressure transducers 2, 4, 5, and 6 are used for stochastic estimation (SE) of system variables.

extremum-seeking control operates correctly. Figure 10 shows the effectiveness of the extremum-seeking control using the SPL spectrogram from the transducer 5. The resonance peak at 2.9 kHz is gradually attenuated and dropped close to the background level, following the reduction of the magnitude ρ^*.

V. Comparison of Extremum-Seeking Control with Fixed-Structure Control

In this section, the performance of the extremum-seeking controller is compared with that of the LQ controller developed by Samimy et al. [2], whose scheme is shown in Fig. 11. The LQ flow control is considered as a representative system in the class of fixed-structure controllers for cavity flow.

A. Overview of Linear-Quadratic Flow Control

The LQ controller is developed on the basis of a fourth-order reduced-order flow model, obtained at Mach 0.30 baseline flow by means of proper orthogonal decomposition (POD) and Galerkin projection methods. The resulting linearized flow model is written as

$$\dot{\mathbf{a}}(t) = G\mathbf{a}(t) + Bu(t) \tag{15}$$

where the vector $\mathbf{a} \in \mathbb{R}^{4\times 1}$ stands for the modal coefficients of the POD expansion. Quadratic stochastic estimation is implemented to correlate real-time measurements of surface pressure fluctuations $P_j(t)$ at m distinct locations with $\mathbf{a}$ in Eq. (15). The estimated states $\hat{a}_i \in \hat{\mathbf{a}}$ are defined as

$$\hat{a}_i(t) = C^{ij}P_j(t) + D^{ijk}P_j(t)P_k(t), \qquad i = 1\cdots 4$$
$$j,k = 1\cdots m \tag{16}$$

In this study, four surface pressure measurements P_2, P_4, P_5, and P_6 in Fig. 11 are selected as feedback signals. The structure of the LQ controller is given by

$$u(t) = -K_{\mathrm{LQ}}\hat{\mathbf{a}}(t) \tag{17}$$

where the gain matrix $K_{\mathrm{LQ}} \in \mathbb{R}^{1\times 4}$ minimizes a quadratic cost function of the system states and the input energy [29]. The major difference between the extremum-seeking controller and the LQ control is the adaptability of the control parameters. The gain matrix K_{LQ} of the LQ controller is determined on the basis of the model identified at a given design condition and is therefore fixed irrespective of the actual flow condition. In contrast, the parameter ϕ of the extremum-seeking control is determined in real time, which in principle yields a means to account for varying flow conditions.

B. Experimental Results

Figure 12 shows a comparison of SPL spectra between the LQ control system and the extremum-seeking control system. In this experiment, the freestream Mach number is set to the design condition of the LQ control system (Mach 0.30). To evaluate the performance of the controllers, we use the pressure fluctuations measured by transducers 2 and 5, which are located, respectively, at the level of the shear layer and at the floor of the cavity. Note that, as opposed to transducer 5, the output of transducer 2 is not used as a feedback signal by the extremum-seeking controller. The SPL spectra corresponding to each transducer are shown in Figs. 12a and 12b. Both control systems show successful and comparable performance: The resonance peaks are significantly reduced, and the overall SPL levels are suppressed to approximately below 120 dB at the shear layer and 110 dB inside the cavity. For the same

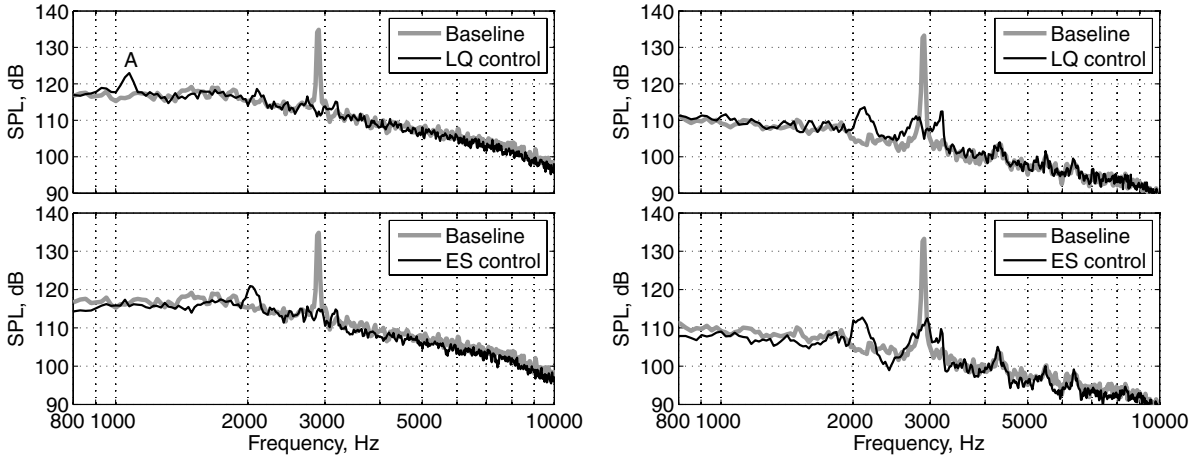

a) Transducer 2 (shear layer) **b) Transducer 5 (bottom of the cavity)**

Fig. 12 SPL spectra from transducers 2 and 5 under LQ control and ES control. The freestream Mach number is 0.30.

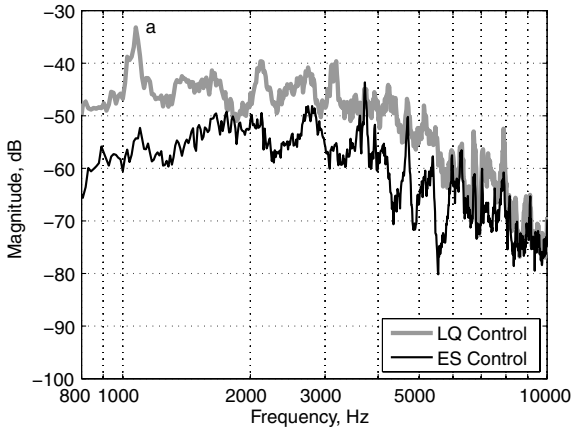

Fig. 13 Frequency spectra of actuator outputs for LQ control and ES control. The freestream Mach number is 0.30.

experiments, the control signals given by the pressure P_i at the actuator output (see Fig. 3) are shown in Fig. 13. The output level of the extremum-seeking control is 10 dB smaller than that of the LQ control. This implies that the extremum-seeking control is more efficient than the LQ control in terms of power consumption. Moreover, the LQ control yields a relatively large peak **a** around 1.1 kHz in Fig. 13. Corresponding to this peak, a peak is detected in the SPL spectrum measured by transducer 2 (peak labeled "A" in Fig. 12a).

The experimental results shown in Figs. 14 and 15 illustrate the performance of each control system at slightly off-design conditions. Although cavity flows at both Mach 0.28 and 0.32 seem to exhibit only one resonance peak, their intrinsic characteristics are quite different. Debiasi and Samimy [5] have shown that the cavity flow at Mach 0.28 belongs to the range of single-resonance mode (Mach 0.25–0.31), whereas the flow at Mach 0.32 is at the lower bound of a range of multiresonance mode (Mach 0.32–0.38). Hence, as shown in Fig. 14, both LQ and extremum-seeking control systems are effective at Mach 0.28, as this case is similar to that of Mach 0.30. The parameter ϕ is adapted from 5.35 at Mach 0.30 to 5.43 at Mach 0.28. In contrast, as shown in Fig. 15, the two control systems exhibit different characteristics as the change of resonance mode becomes imminent at Mach 0.32. The performance of the LQ control starts deteriorating. The resonance peak is still suppressed, but a relatively large spurious peak is created at around 2.2 kHz. On the other hand, the extremum-seeking control maintains a level of performance similar to the results obtained at Mach 0.28 and 0.30 flows. The parameter ϕ is tuned to 2.58, a significantly different value

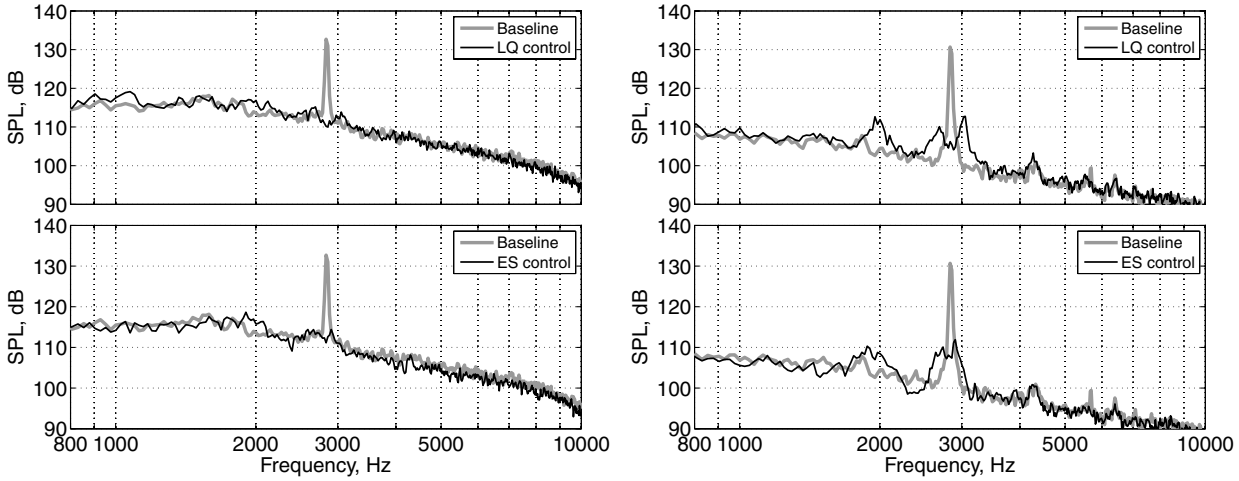

a) Transducer 2 (shear layer) **b) Transducer 5 (bottom of the cavity)**

Fig. 14 SPL spectra from transducers 2 and 5 under LQ control and ES control. The freestream Mach number is 0.28.

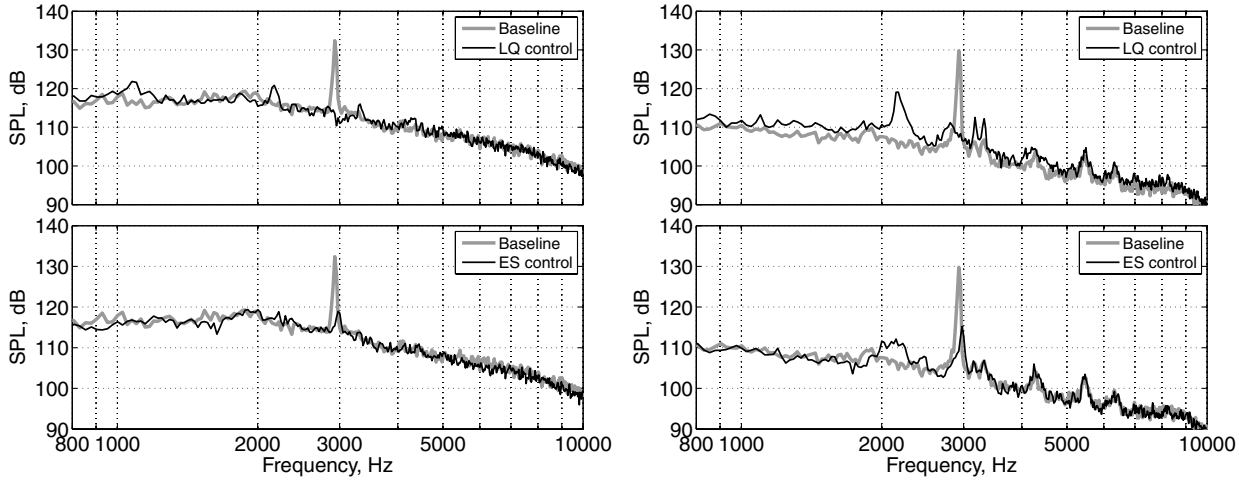

a) Transducer 2 (shear layer) **b) Transducer 5 (bottom of the cavity)**

Fig. 15 SPL spectra from transducers 2 and 5 under LQ control and ES control. The freestream Mach number is 0.32.

due to the variation of the cavity flow dynamics occurring between Mach 0.30 and 0.32 flows.

As seen in Figs. 16 and 17, as the Mach number increases further beyond 0.32, multiple resonance peaks are observed in the SPL spectra (two peaks in these experiments). At this range of Mach numbers, the LQ control significantly amplifies the peak at 2.2 kHz, even though it attenuates the second peak of the baseline flow. In addition, the background pressure fluctuation level below 2 kHz tends to increase. The extremum-seeking control is relatively more effective compared to the LQ system. The extremum-seeking control succeeds in suppressing the larger peak between the two peaks of the baseline flow, that is, the 3.4 kHz peak at Mach 0.34 and the 2.5 kHz peak at Mach 0.38, while it barely affects the magnitude of the smaller peak. However, it does not generate any side effect, as opposed to the LQ control. It is worth noting that the behavior of the extremum-seeking control, which tends to suppress the largest peak, is consistent with the fact that the algorithm does not possess any information on the frequency of the limit cycle. This also suggests that the current single-parameter adaptive scheme is not sufficient for handling a multiresonance mode, and a multiparameter scheme would be required instead. Listed here are the variations of ϕ with respect to different Mach numbers as follows: Mach 0.28, $\phi = 5.43$; Mach 0.30, $\phi = 5.35$; Mach 0.32, $\phi = 2.58$; Mach 0.34, $\phi = 2.33$; and Mach 0.38, $\phi = 2.45$. The large difference between Mach 0.30 and 0.32 indicates that the extremum-seeking control system successfully adapts itself to the change of cavity flow resonance from single mode to multiple modes, even though it cannot completely suppress multiple resonances.

Finally, Fig. 18a compares the root-mean-squared (rms) magnitudes of the actuator voltage input for each control system. This plot facilitates assessing the efficiency of each control system with respect to cavity flow Mach number. The LQ control applies increasingly larger voltage signals to the actuator as the Mach number deviates from the design Mach number 0.30 to higher numbers. In contrast, the extremum-seeking control needs smaller voltage magnitude, which is maintained within a small range in spite of significant change in Mach number. Figure 18b shows the change of the overall sound pressure level (OASPL) of the controlled flow with respect to the baseline flow, which is denoted by ΔOASPL and defined as follows:

$$\Delta\text{OASPL} = \text{OASPL}_{\text{controlled flow}} - \text{OASPL}_{\text{baseline}}$$

with

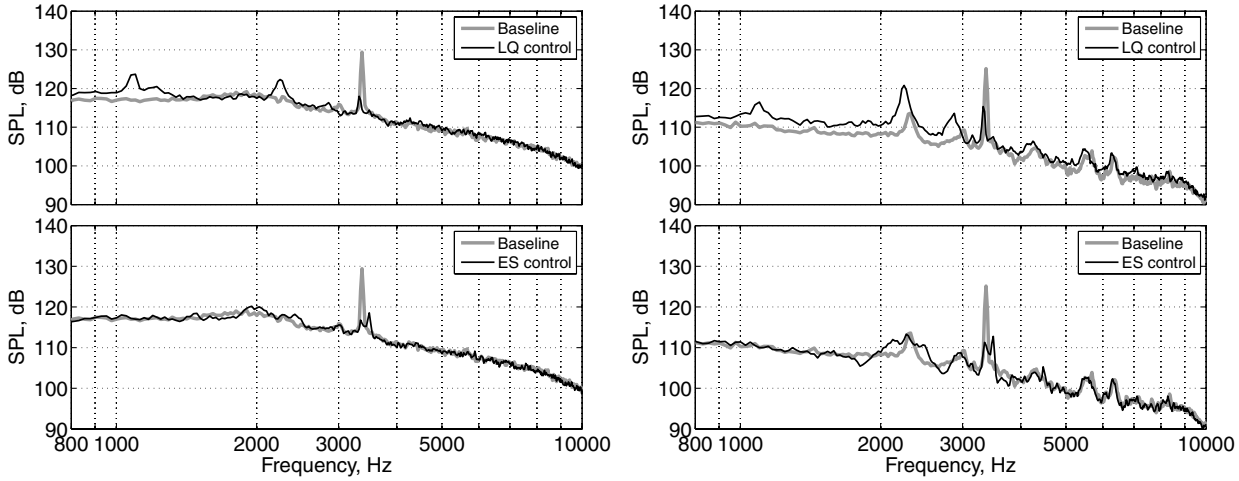

a) Transducer 2 (shear layer) **b) Transducer 5 (bottom of the cavity)**

Fig. 16 SPL spectra from transducers 2 and 5 under LQ control and ES control. The freestream Mach number is 0.34.

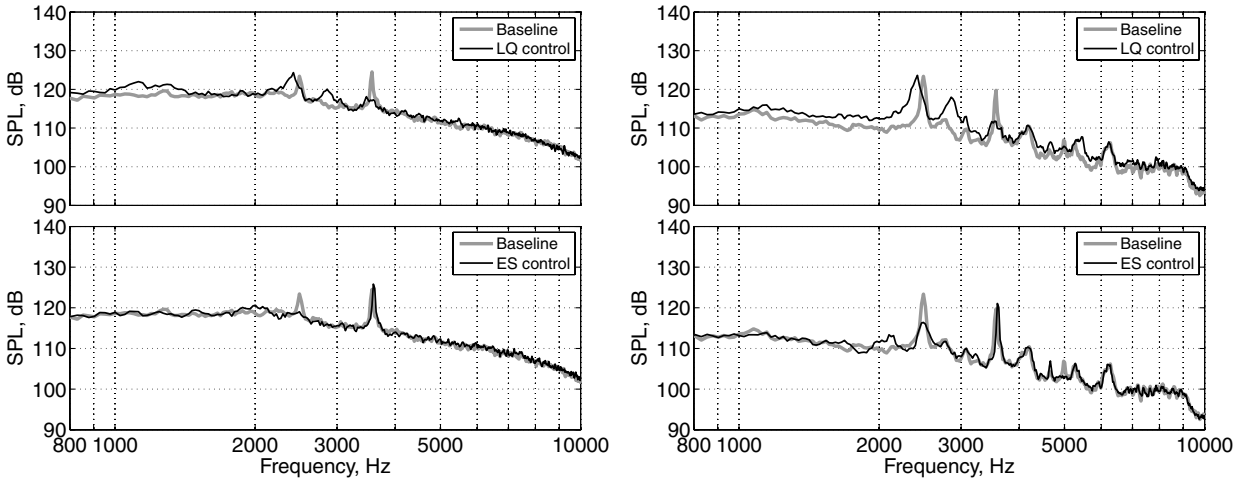

a) Transducer 2 (shear layer) **b) Transducer 5 (bottom of the cavity)**

Fig. 17 SPL spectra from transducers 2 and 5 under LQ control and ES control. The freestream Mach number is 0.38.

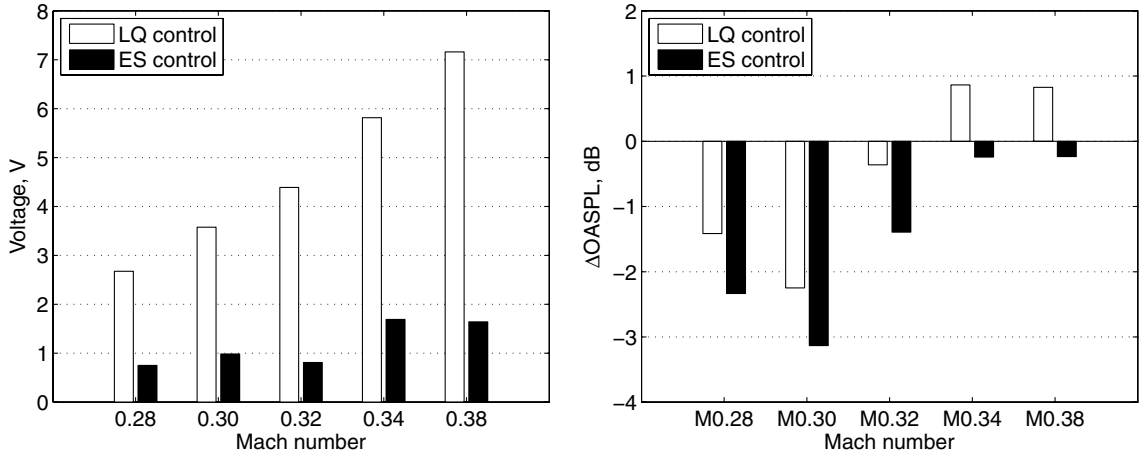

a) RMS magnitude of actuator input **b) Change of overall SPL (ΔOASPL.)**

Fig. 18 Comparison of Extremum-seeking control and LQ control in terms of actuator voltage input and overall SPL for different Mach numbers.

$$\text{OASPL} = 10\log_{10}\frac{\bar{P}_{\text{rms}}^2}{P_o^2}, \qquad \bar{P}_{\text{rms}} = \frac{1}{m}\sum_{j=1}^{m} P_{\text{rms},j}$$

$$P_{\text{rms},j} = \sqrt{\frac{1}{n}\sum_{k=1}^{n}|P_j(k)|^2}$$

where the reference pressure is $P_o = 20\ \mu$Pa, and the number of pressure measurement locations is $m = 6$. The value of ΔOASPL is considered as an overall performance indicator of the flow control system. The trend in ΔOASPL with respect to Mach number shows the clear advantage of extremum-seeking control over fixed-structure control systems. Although the LQ control is beneficial only in design condition (Mach 0.30) and its neighborhood (Mach 0.28 and 0.32), the extremum-seeking control shows better performance at single-resonance modes than the LQ control and maintains its effectiveness to some degree even at multiresonance modes.

VI. Conclusions

A varying flow condition in a subsonic shallow cavity flow often significantly affects the dynamic characteristics of cavity flow resonance. In our configuration, increasing the Mach number from 0.30 to 0.38 changes the resonance from a single mode to multiple modes. In the present work, we developed an adaptive flow control system using an extremum-seeking algorithm, which aims at adapting the control parameters to maximize the attenuation of the flow resonance at various flow conditions. An inner closed-loop control system was developed using a simple, pressure-based control law. The effects of the control parameters, that is, gain K and phase ϕ, on the limit cycle magnitude ρ were identified analytically and experimentally. It was verified from both analytical relationships and experimental results that there exists an optimal value ϕ_{opt} of the controller parameter where ρ is minimized, regardless of K. As for the effects of K, the analytical prediction does not match the experimental results, due to the simplicity of a phasor model derived from a Galerkin system. Therefore, extremum-seeking optimization was applied only to the parameter ϕ, with the parameter K fixed. A gradient-based searching algorithm with a sinusoidal perturbation was implemented as an optimization scheme. The effectiveness of the extremum-seeking control was verified under various flow Mach numbers. The experimental results were compared with those obtained with a linear-quadratic feedback control based on a reduced-order Galerkin model representing a class of fixed-structure control systems. Although the LQ control attenuates the resonance only at Mach numbers close to the design condition, the extremum-seeking control extends the range of Mach numbers where the control is effective by tuning the control parameter automatically.

Acknowledgments

This work was supported in part by the U.S. Air Force Research Laboratories/Air Vehicles Directorate and the U.S. Air Force Office of Scientific Research through the Collaborative Center of Control Science (CCCS) (Contract F33615-01-2-3154). The authors would like to thank their colleagues at CCCS, James Myatt, Chris Camphouse, Edgar Caraballo, and Jesse Little for assistance and fruitful discussions.

References

[1] Gad-el-Hak, M., *Flow Control: Passive, Active, and Reactive Flow Management*, Cambridge Univ. Press, New York, 2004.

[2] Samimy, M., Debiasi, M., Caraballo, E., Serrani, A., Yuan, X., Little, J., and Myatt, J. H., "Feedback Control of Subsonic Cavity Flows Using Reduced-Order Models," *Journal of Fluid Mechanics*, Vol. 579, May 2007, pp. 315–346. doi:10.1017/S0022112007005204

[3] Rowley, C., and Williams, D. R., "Dynamics and Control of High-Reynolds-Number Flow over Open Cavities," *Annual Review of Fluid Mechanics*, Vol. 38, Jan. 2006, pp. 251–276. doi:10.1146/annurev.fluid.38.050304.092057

[4] Cattafesta, L. N., Williams, D. R., Rowley, C. W., and Alvi, F. S., "Review of Active Control of Flow-Induced Cavity Resonance," AIAA Paper 2003-3567, 2003.

[5] Debiasi, M., and Samimy, M., "Logic-Based Active Control of Subsonic Cavity Flow Resonance," *AIAA Journal*, Vol. 42, No. 9, Sept. 2004, pp. 1901–1909. doi:10.2514/1.4799

[6] Yan, P., Debiasi, M., Yuan, X., Little, J., Özbay, H., and Samimy, M., "Experimental Study of Linear Closed-Loop Control of Subsonic Cavity Flow," *AIAA Journal*, Vol. 44, No. 5, 2006, pp. 929–938. doi:10.2514/1.14873

[7] Efe, M. Ö., Debiasi, M., Yan, P., Özbay, H., and Samimy, M., "Neural Network Based Modeling of Subsonic Cavity Flows," *International Journal of Systems Science*, Vol. 39, No. 2, Feb. 2008, pp. 105–117. doi:10.1080/00207720701726188

[8] Ariyur, K. B., and Krstić, M., *Real-Time Optimization by Extremum-Seeking Control*, Wiley, Hoboken, NJ, 2003.

[9] Åström, K. J., and Wittermark, B., *Adaptive Control*, Electrical and Computer Engineering, Addison-Wesley, Reading, MA, 2nd ed., 1995.

[10] Leyva, R., Alonso, C., Queinnec, I., Cid-Pastor, A., Lagrange, D., and Martinez-Salamero, L., "MPPT of Photovoltaic Systems Using Extremum-Seeking Control," *IEEE Transactions on Aerospace and Electronic Systems*, Vol. 42, No. 1, Jan. 2006, pp. 249–258. doi:10.1109/TAES.2006.1603420

[11] Guelman, M., Kogan, A., Kazarian, A., Livne, A., Orenstein, M., and Michalik, H., "Acquisition and Pointing Control for Inter-Satellite Laser Communications," *IEEE Transactions on Aerospace and Electronic Systems*, Vol. 40, No. 4, Oct. 2004, pp. 1239–1248. doi:10.1109/TAES.2004.1386877

[12] Zhang, C., and Ordonez, R., "Numerical Optimization-Based Extremum Seeking Control with Application to ABS Design," *IEEE*

Transactions on Automatic Control, Vol. 52, No. 3, March 2007, pp. 454–467.
doi:10.1109/TAC.2007.892389

[13] Li, Y., Rotea, M., Chiu, G.-C., Mongeau, L., and Paek, I.-S., "Extremum Seeking Control of a Tunable Thermoacoustic Cooler," *IEEE Transactions on Control Systems Technology*, Vol. 13, No. 4, July 2005, pp. 527–536.
doi:10.1109/TCST.2005.847334

[14] Popovic, D., Jankovic, M., Magner, S., and Teel, A., "Extremum Seeking Methods for Optimization of Variable Cam Timing Engine Operation," *IEEE Transactions on Control Systems Technology*, Vol. 14, No. 3, May 2006, pp. 398–407.
doi:10.1109/TCST.2005.863660

[15] Banaszuk, A., Ariyur, K. B., Krstić, M., and Jacobson, C. A., "An Adaptive Algorithm for Control of Combustion Instability," *Automatica*, Vol. 40, No. 11, 2004, pp. 1965–1972.
doi:10.1016/j.automatica.2004.06.008

[16] Wang, H.-H., Yeung, S., and Krstić, M., "Experimental Application of Extremum Seeking on an Axial-Flow Compressor," *IEEE Transactions on Control Systems Technology*, Vol. 8, No. 2, 2000, pp. 300–309.
doi:10.1109/87.826801

[17] Banaszuk, A., and Narayanan, S., "Adaptive Control of Flow Separation in a Planar Diffuser," AIAA Paper 2003-0617, 2003.

[18] Garwon, M., and King, R., "A Multivariable Adaptive Control Strategy to Regulate the Separated Flow Behind a Backward-Facing Step," *Proceedings of the 16th IFAC World Congress*, International Federation of Automatic Control, Laxenburg, Austria, 2005.

[19] Henning, L., and King, R., "Drag Reduction by Closed-Loop Control of a Separated Flow over a Bluff Body with a Blunt Trailing Edge," *Proceedings of the 44th IEEE Conference on Decision and Control and European Control Conference*, IEEE, Piscataway, NJ, 2005, pp. 494–499.

[20] Beaudoin, J.-F., Cadot, O., Aider, J.-L., and Wesfried, J.-E., "Drag Reduction of a Bluff Body Using Adaptive Control Methods," *Physics of Fluids*, Vol. 18, No. 8, 2006, pp. 085107-1–085107-10.
doi:10.1063/1.2236305

[21] Becker, R., King, R., Petz, R., and Nitsche, W., "Adaptive Closed-Loop Separation Control on a High-Lift Configuration Using Extremum Seeking," *AIAA Journal*, Vol. 45, No. 6, 2007, pp. 1382–1392.
doi:10.2514/1.24941

[22] Tadmor, G., Noack, B. R., Morzyński, M., and Siegel, S., "Low-Dimensional Models for Feedback Flow Control. Part 2: Control Design and Dynamic Estimation," AIAA Paper 2004-2409, 2004.

[23] Rowley, C. W., and Juttijudata, V., "Model-Based Control and Estimation of Cavity Flow Oscillations," *Proceedings of the 44th IEEE Conference on Decision and Control*, IEEE, Piscataway, NJ, 2005, pp. 512–517.

[24] Wang, H.-H., and Krstić, M., "Extremum Seeking for Limit Cycle Minimization," *IEEE Transactions on Automatic Control*, Vol. 45, No. 12, 2000, pp. 2432–2437.
doi:10.1109/9.895589

[25] Kim, K., Debiasi, M., Schultz, R., Serrani, A., and Samimy, M., "Dynamic Compensation of a Synthetic Jet-Like Actuator for Closed-Loop Cavity Flow Control," *AIAA Journal*, Vol. 46, Jan. 2008, pp. 232–240.
doi:10.2514/1.30095

[26] Kasnakoğlu, C., and Serrani, A., "Attenuation of Oscillations in Galerkin Systems Using Center-Manifold Techniques," *European Journal of Control*, Vol. 13, No. 5, 2007, pp. 529–542.
doi:10.3166/ejc.13.529-542

[27] Guckenheimer, J., and Holmes, P., *Nonlinear Oscillations, Dynamical Systems, and Bifurcations of Vector Fields*, Vol. 42, Applied Mathematical Sciences, Springer, New York, 3rd ed., 1983.

[28] Bendat, J. S., and Piersol, A. G., *Random Data: Analysis and Measurement Procedures*, Wiley, New York, 2000.

[29] Skogestad, S., and Postlethwaite, I., *Multivariable Feedback Control*, Wiley, West Sussex, England, 2nd ed., 2005.

J. Wei
Associate Editor